Journal of Energy Chemistry 72 (2022) 258–264

Contents lists available at ScienceDirect

Journal of Energy Chemistry

journal homepage: www.elsevier.com/locate/jechem

http://www.journals.elsevier.com/journal-of-energy-chemistry/

Dynamic chemical processes on ZnO surfaces tuned by physisorption under ambient conditions

Yunjian Ling [a,d,1], Jie Luo [b,1], Yihua Ran [c], Yunjun Cao [a], Wugen Huang [a,d], Jun Cai [c], Zhi Liu [c], Wei-Xue Li [b,*], Fan Yang [a,c,*], Xinhe Bao [a]

[a] State Key Laboratory of Catalysis, Dalian Institute of Chemical Physics, Chinese Academy of Sciences, Dalian 116023, Liaoning, China
[b] School of Chemistry and Materials Science, Hefei National Laboratory for Physical Sciences at Microscales, University of Science and Technology of China, Hefei 230026, Anhui, China
[c] School of Physical Science and Technology, ShanghaiTech University, Shanghai 201210, China
[d] University of Chinese Academy of Sciences, Beijing 100039, China

ARTICLE INFO

Article history:
Received 1 March 2022
Accepted 7 March 2022
Available online 15 March 2022

Keywords:
Dynamic chemical processes
Zinc oxide
Physisorption
Ambient-pressure STM
DFT

ABSTRACT

The catalytic properties of non-reducible metal oxides have intrigued continuous interest in the past decades. Often time, catalytic studies of bulk non-reducible oxides focused on their high-temperature applications owing to their weak interaction with small molecules. Hereby, combining ambient-pressure scanning tunneling microscopy (AP-STM), AP X-ray photoelectron spectroscopy (AP-XPS) and density functional theory (DFT) calculations, we studied the activation of CO and CO_2 on ZnO, a typical non-reducible oxide and major catalytic material in the conversion of C1 molecules. By visualizing the chemical processes on ZnO surfaces at the atomic scale under AP conditions, we showed that new adsorbate structures induced by the enhanced physisorption and the concerted interaction of physisorbed molecules could facilitate the activation of CO and CO_2 on ZnO. The reactivity of ZnO towards CO could be observed under AP conditions, where an ordered (2×1)–CO structure was observed on ZnO$(10\bar{1}0)$. Meanwhile, chemisorption of CO_2 on ZnO$(10\bar{1}0)$ under AP conditions was also enhanced by physisorbed CO_2, which minimizes the repulsion between surface dipoles and causes a (3×1)–CO_2 structure. Our study has brought molecular insight into the fundamental chemistry and catalytic properties of ZnO surfaces under realistic reaction conditions.

1 Introduction

The adsorption and reaction of molecules over oxide surfaces are essential for understanding the functions of metal oxides, which are of center interest to many areas of chemistry, physics, materials science and geology [1]. As the surface chemistry of reducible oxides is often attributed to the presence of oxygen defects [2,3], the origin of catalytic properties of non-reducible oxides has remained to be explored despite their wide applications in catalysis [4,5]. To understand their surface chemistry, fundamental studies have been dedicated to the adsorption of small molecules on non-reducible oxide surfaces [6], which were mostly performed in ultrahigh vacuum (UHV) at cryogenic temperatures owing to their weak interaction with small molecules.

In the past decades, the development of ambient-pressure (AP) surface science techniques has demonstrated on metal surfaces [7–12], that rich dynamic processes could be observed under AP conditions that do not occur in UHV, but are responsible for the catalytic properties of metal catalysts. Much less attention has been devoted to the atomic-scale adsorption and reaction processes on oxide surfaces under realistic reaction conditions, which in part could be attributed to the experimental difficulties of AP characterization on oxide surfaces with atomic resolution [13]. For instance, AP scanning tunneling microscopy (AP-STM) studies on bulk oxide surfaces have been challenging because of the difficulties to maintain a stable tunneling junction [14] on semiconductors in a reactive environment. Here, by improving the stability of AP-STM, we can now visualize the atomic-scale dynamics of oxide surfaces in response to ambient reactant gases. We show that the surfaces of non-reducible oxides could exhibit reactivity at even low temperatures [15]. In contrast to the chemisorption-induced processes on metals, the collective interaction of physisorbed molecules was

* Corresponding authors.
E-mail addresses: wxli70@ustc.edu.cn (W.-X. Li), fyang@shanghaitech.edu.cn (F. Yang).
[1] These authors contributed equally to this work.

https://doi.org/10.1016/j.jechem.2022.03.009

found to enhance their activity and result in dynamic chemical processes on non-reducible oxide surfaces.

ZnO is one of the most used oxide materials for energy conversion and environmental remediation [16]. In catalysis, ZnO-based catalysts are key to methanol synthesis [17], syngas conversion [18], steam reforming [19] and water–gas shift reaction [20], which are major processes of the methanol economy and hydrogen economy. Extensive efforts have been dedicated to studying the surface structure [21,22] and surface chemistry [23–28] of ZnO. However, as a non-reducible oxide, the ZnO surface exhibited little reactivity in UHV due to its weak interaction with small molecules. So far, there has been a lack of atomic-scale studies to understand molecular activation processes on ZnO under realistic ambient conditions.

Hereby, we combined AP-STM, AP X-ray photoelectron spectroscopy (AP-XPS) and density functional theory (DFT) calculations to study the adsorption and activation of CO and CO_2 on ZnO($10\bar{1}0$), which is the most stable surface of ZnO [29]. While CO does not adsorb on ZnO($10\bar{1}0$) in UHV at 300 K, we found that physisorption of CO on ZnO($10\bar{1}0$) under AP conditions could cause the reaction between CO and lattice oxygen of ZnO to form CO_2. The collective interaction of weakly adsorbed molecules also modulates strong chemisorption and resulted in a new adsorbate structure of CO_2 on ZnO. By visualizing the dynamic chemical processes of CO and CO_2 on ZnO($10\bar{1}0$), our study has brought molecular insight for fundamental C1 chemistry over ZnO surfaces.

2 Experimental

2.1 Model catalyst preparation and characterization

A customized STM system was employed which contains a sample preparation chamber and a NAP-STM (SPECS, base pressure < 3×10^{-10} mbar) with a near-ambient pressure (NAP) cell [30]. AP-XPS studies were performed using a customized AP-XPS systems (SPECS, base pressure < 8×10^{-10} mbar), equipped with a monochromic Al Kα X-ray source and a hemispherical energy analyzer (PHOIBOS) [31]. ZnO($10\bar{1}0$) (purchased from MatecK) were treated by 2–3 cycles of Ar^+ sputtering (1 keV 10 μA) and subsequent annealing at ∼ 1100 K to remove possible impurities. For the final annealing step, the annealing temperature was reduced to ∼ 900 K to obtain a defect-free surface. CO gas was purified in liquid N_2 cold trap for over half an hour and then introduced to the NAP cell. For experiments at elevated temperatures, STM scanning was performed during the cooling of ZnO($10\bar{1}0$) to near room temperature. STM images were obtained using Pt/Ir tips and processed with SPIP (Image Metrology, Denmark).

2.2 Computational methods

Density functional theory (DFT) calculations were performed by Vienna ab initio simulation package (VASP) using PAW potential [32–34], and the exchange–correlation interaction was described via the optB86b-vdW functional [35], the electronic analysis was calculated by Perdew–Burke–Ernzerhof (PBE) exchange–correlation functional [36]. As shown previously [37,38], the method used (DFT, DFT + U) has little influence on the description of binding energy and reaction barriers. The plane wave basis set with a kinetic energy cutoff of 400 eV was used to solve the Kohn-Sham equations. The optimized lattice constants of bulk wurtzite ZnO are $a = b = 3.29$ Å with $c = 5.30$ Å, which are consistent with the experimental results ($a = b = 3.25$ Å with $c = 5.21$ Å) [39,40]. ZnO($10\bar{1}0$) surfaces were modeled by a three double layer slab model separated by 12 Å vacuum along Z-direction. The ($2 \times 2 \times 1$) and ($3 \times 2 \times 1$) k-point mesh were used to sample the Brillouin zone for (3×2) and (2×2) periodicity slab models. The bottom-one layer of the slab was fixed and the remaining atoms were relaxed until the residual forces were less than 0.02 eV/ Å. The <0001> step was simulated by the ZnO($13\bar{4}0$) surface which was modeled by a three layer slab model separated by 12 Å vacuum along Z-direction. The ($2 \times 2 \times 1$) k-point mesh was used to sample the Brillouin zone for (1×2) periodicity slab model. The climbing-image nudged elastic band (CI-NEB) method [41,42] was carried out to identify the transition states, and then verified to possess only one vibrational mode with a negative curvature in the direction of bond breaking or forming process. The STM images were simulated on the basis of Tersoff and Hamann's formula [43–45] using the bSKAN code [46–48].

3 Results and discussion

3.1 Structure of the ZnO($10\bar{1}0$) surface

The pristine surface of ZnO($10\bar{1}0$) was prepared by the procedure described in Experimental section and exhibits flat terraces with straight step edges running along the [0001] and [$1\bar{2}10$] directions (Fig. 1a). Unlike the surfaces of reducible transition metal oxides, point defects were scarce on ZnO($10\bar{1}0$) with surface concentration < 1%. From STM, the bright rows on the surface terrace of ZnO($10\bar{1}0$) run along the [$1\bar{2}10$] direction were attributed as Zn rows [21]. Atomically resolved STM image (Fig. 1b) shows that the ZnO($10\bar{1}0$) surface exhibits a rectangular unit cell, with cell lengths of 3.26 Å along the [$1\bar{2}10$] direction and 5.29 Å along the [0001] direction, respectively. The simulated STM image based on the DFT-optimized ZnO($10\bar{1}0$) showed further that the topmost Zn atoms along the [$1\bar{2}10$] direction were resolved as bright spots, whereas neighboring O atoms were resolved as depressions (Fig. 1c). From the projected density of states (PDOS, Fig. S1), both O and Zn exhibit empty states in the conduction band near the Fermi level. But, the unoccupied PDOS of Zn is considerably higher than that of O, resulting in the bright contrast of Zn atoms in the STM image.

3.2 CO adsorption and reaction on ZnO($10\bar{1}0$)

Although CO would desorb from the ZnO surface at 300 K in UHV, physisorption of CO on ZnO($10\bar{1}0$) under ambient conditions was found to form a well-ordered two-dimensional adsorbate phase across the surface terrace. Fig. 2(a) shows that, when 1 mbar CO was introduced at 300 K, a well-ordered (2×1) adsorbate phase could be observed on ZnO($10\bar{1}0$) and covered fully the surface terrace. The adsorption geometry of CO has been studied previously at cryogenic temperatures in UHV [29,49,50], which suggested that CO binds to the surface Zn^{2+} site and is orientated at 30 degrees off to the surface normal.

Our DFT calculations showed that CO molecules bind to surface Zn^{2+} sites of ZnO($10\bar{1}0$) with a saturation surface coverage of 1/2 ML and give an average adsorption energy of CO at −0.58 eV/CO. DFT-based STM simulation (Fig. 2b) suggested that CO molecules appear as bright dots on ZnO($10\bar{1}0$) since from PDOS (Fig. S2a), $2\pi^*$ antibonding states of CO (LUMO) dominate the conduction band at near the Fermi level, which exhibits a similar shape as those of gas phase CO molecules (Fig. S2b). CO molecules were found to adsorb continuously along the [0001] direction, but at intervals along the [$1\bar{2}10$] direction, forming a (2×1)–CO structure on ZnO($10\bar{1}0$) and consistent with STM observation. When the coverage of CO increases to 1 ML, the average adsorption

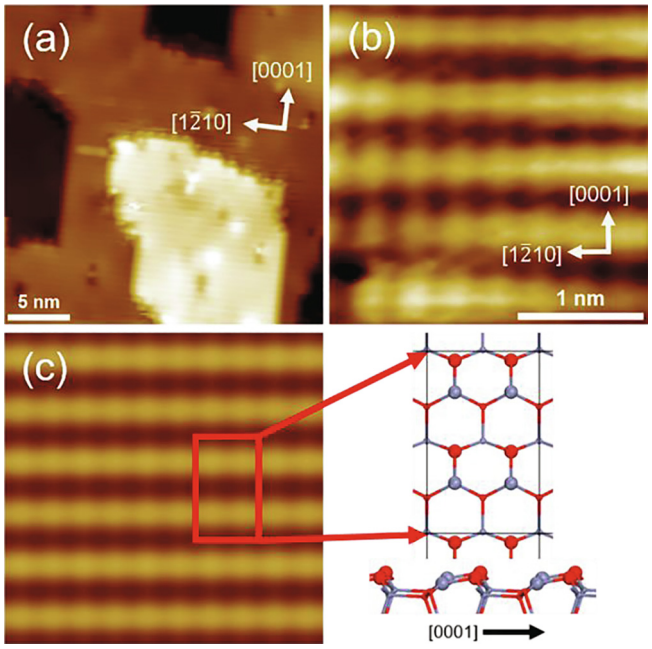

Fig. 1. Surface Structure of ZnO(10$\bar{1}$0). (a) Large-scale, (b) atomically-resolved and (c) simulated STM images of clean ZnO(10$\bar{1}$0). The bright spots in (b) are surface Zn atoms along the [1$\bar{2}$10] direction. The corresponding structure of ZnO(10$\bar{1}$0) is displayed on the right side of the simulated image (c). Scanning parameters: (a) U = 2.4 V, I_t = 90 pA; (b) U = 1.1 V, I_t = 300 pA. Gray and red spheres represent Zn and O atoms, respectively.

energy of CO is −0.53 eV/CO, implying that there is weak repulsion between adjacent CO along the [1$\bar{2}$10] direction. Gibbs free energies were further calculated to identify the adsorption structure of CO at varying temperatures and pressures (Fig. S3) and confirm the formation of (2 × 1)–CO structure under AP conditions at 300 K.

Despite the weak interaction between CO and ZnO(10$\bar{1}$0), our study found that these physisorbed CO could react with the lattice oxygen of ZnO. Fig. 2(c) showed that there are extra bright spots scattering across the surface and located at the center of the (2 × 1) cell. These bright spots could be assigned to CO_2 species formed via the reaction between CO and ZnO (Fig. 2d), which was also evident from STM simulation and AP-XPS measurement at 300 K (Fig. 2e and f). In 0.5 mbar CO, C 1 *s* spectra showed a shoulder peak at 290.1 eV besides the large gas phase CO peak, indicating the formation of CO_2 species which increase at 400 K. Note that, CO oxidation is known to occur at the ZnO-Pt(111) interface, where chemisorbed CO reacted with oxygen at interfacial sites [5]. Hereby, we found that physisorbed CO on ZnO could also react with lattice oxygen of ZnO, although at a much slower rate. In the CO atmosphere, in-situ STM showed that the bright spots, CO_2 adsorbates, could diffuse facilely along the <1$\bar{2}$10> and <0001> directions (Fig. S4), which also ruled out the possibility of bright spots being surface defects, because lattice atoms of oxide surfaces are usually lack of diffusivity at room temperature [51]. Upon the evacuation of CO gas, the adsorbate structure and bright spots both disappeared, indicating the bright spots are reaction products, rather than surface oxygen vacancies on ZnO. Note that, STM studies have suggested that oxygen defects on ZnO(10$\bar{1}$0) appeared as dark features [52,53]. Meanwhile, a small amount of CO_2 adsorbates were observed on bare ZnO as carbonate species upon evacuation and appeared as dark lines [54] (Fig. S5).

The reaction between physisorbed CO and lattice oxygen of ZnO(10$\bar{1}$0) could be further evidenced by AP-STM measurements at elevated temperatures (Fig. 3). When ZnO(10$\bar{1}$0) was annealed in 1 mbar CO at 500 K in the STM cell and then cooled

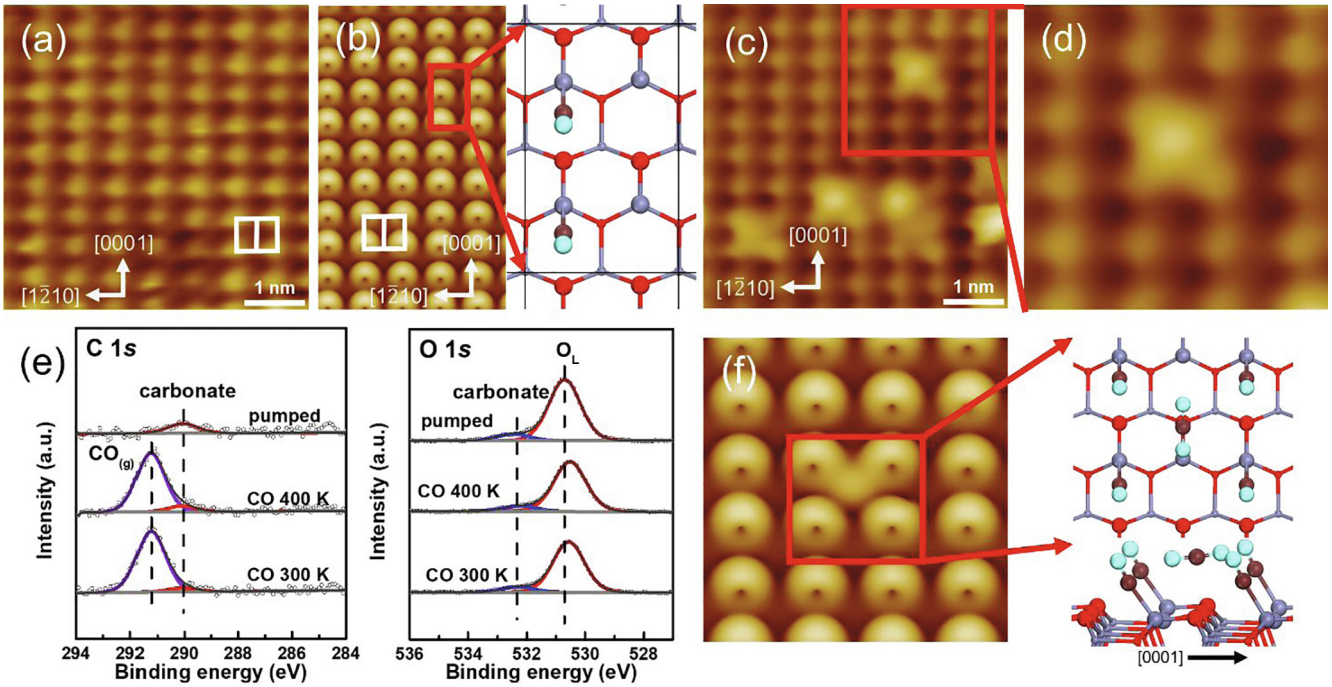

Fig. 2. Adsorption and reaction of CO on ZnO (10$\bar{1}$0) under ambient conditions. (a–d) STM images and STM simulation of ZnO(10$\bar{1}$0) in 1 mbar CO at room temperature. The formation of (2 × 1)–CO structure is calculated by DFT with the optimized structural model and simulated STM image depicted in (b), showing 1/2 ML CO adsorbed on ZnO(10$\bar{1}$0). The (2 × 1)–CO structure is magnified in (c) showing the presence of bright spots within the (2 × 1) unit cell. The bright spots are diffusing during the imaging process and could be assigned as CO_2 species. The area marked in (c) is highlighted in (d). The white rectangles represent surface Zn lattice. (e) AP-XPS C 1 *s* and O 1 *s* of ZnO(10$\bar{1}$0) in 0.5 mbar CO or after the evacuation of CO gas. (f) Simulated STM image and the corresponding structural model of CO_2 adsorption in the (2 × 1)–CO structure on ZnO(10$\bar{1}$0). Scanning parameters: (a) U = 2.4 V, I_t = 120 pA; (c, d) U = 2.4 V, I_t = 130 pA. Gray, red, green and brown spheres represent Zn, lattice O, O in adsorbents and C atoms, respectively. (For interpretation of the references to colour in this figure legend, the reader is referred to the web version of this article.)

to ~ 300 K for AP-STM measurements, the surface concentration of bright spots (CO_2 adsorbates) was found to increase significantly (Fig. 3a), which also ruled out the possibility of bright spots from impurities in CO gas (Fig. 2e). Background contamination, such as H_2O, in our AP-STM studies typically occurred during elongated measurements, but not spontaneously, and thus not consistent with the above observation.

A piece of conclusive evidence for the reaction between physisorbed CO and lattice oxygen of ZnO($10\bar{1}0$) is demonstrated by the etching of step edges (Fig. 3b), especially along the <0001> step with alternating Zn and O terminating atoms. Zn-O dimer vacancies (Fig. 3c) were observed continuously along the <0001> step and dispersed along the <$1\bar{2}10$> direction. The removal of edge O atoms by CO reaction caused the simultaneous evaporation or bulk diffusion of Zn atoms at neighboring sites at elevated temperatures, leading to the formation of corroded edge shapes. DFT calculations showed that the reaction energy between CO and O at the <0001> step is −0.62 eV, more exothermic than that between CO and O on the surface terrace of ZnO (-0.19 eV). The reaction diagram of CO reacting with the <0001> step is depicted in Fig. 3(d), showing that the reaction between CO and lattice oxygen needs to overcome a barrier of 0.46 eV to form CO_2. The low reaction barrier suggests that CO can easily bond with surface oxygen [55]. By overcoming an energy barrier of 0.40 eV, CO_2 formed could desorb from ZnO($10\bar{1}0$) with an oxygen vacancy left behind. The CO_2 molecule could also diffuse and adsorb on the surface terrace to form a tridentate carbonate. Thus, physisorbed CO could react with the lattice oxygen of ZnO at 300 K, in addition to the formation of an ordered (2 × 1)–CO phase. The adsorption/desorption states of CO_2 are also modulated by ambient CO, as well as its diffusion kinetics.

3.3 CO_2 adsorption on ZnO($10\bar{1}0$)

The adsorption of CO_2 on oxides is typically a strong chemisorption process and could be readily studied in UHV. Previous studies have shown that a (2 × 1)–CO_2 structure could be observed in UHV on ZnO($10\bar{1}0$) [54]. Consistently, we observed the (2 × 1)–CO_2 structure when ZnO($10\bar{1}0$) was exposed to 1 × 10^{-5} mbar CO_2 at 300 K (Fig. S6a, 4a), which gave a surface coverage of 0.5 ML CO_2. The corresponding structural model and STM simulation (Fig. 4b and c) depicted the formation of tridentate carbonate along the [0001] direction of ZnO($10\bar{1}0$). In UHV, the (2 × 1)–CO_2 phase with tridentate adsorption configuration is attributed to the most stable structure of chemisorbed CO_2 on ZnO and gives an average adsorption energy at −1.28 eV/CO_2. Note that, the (2 × 1) adsorbate structures of CO_2 and CO could be distinguished from their desorption behavior (Fig. S5). Upon the evacuation of CO gases, CO adsorbates would desorb completely from the ZnO($10\bar{1}0$) surface for its weak binding energy (-0.58 eV/CO), whereas the evacuation of CO_2 gases would only cause partial desorption of CO_2, leaving chemisorbed CO_2 chains on ZnO($10\bar{1}0$). In the case of CO reaction with ZnO($10\bar{1}0$), the evacuation of CO gas could leave a surface with chemisorbed CO_2.

In comparison, a new adsorbate phase could be observed under ambient-pressure CO_2 (Fig. S6b). The formation of an ordered (3 × 1)–CO_2 structure is spontaneous on ZnO($10\bar{1}0$) and covers the whole surface terrace upon the exposure of 3 mbar CO_2. Similar to CO_2 adsorption in UHV, CO_2 adsorbate chains run along the [0001] direction in the (3 × 1)–CO_2 phase (Fig. 4d). But, the (3 × 1) structure in ambient CO_2 is expected to have a higher CO_2 density than the (2 × 1) phase (0.5 ML) in UHV. DFT calculations compared the adsorption structures of CO_2 at different coverages. The (3 × 1) phase observed above corresponds to the surface fully covered by CO_2 (1 ML). Within the (3 × 1) structure, 1/3 of CO_2 molecules are physisorbed through weak van der Waals interaction between adsorbates and ZnO while the remaining 2/3 ML of CO_2 molecules exhibit stronger chemical adsorption on ZnO. The (3 × 1)–CO_2 phase is a dynamically stabilized structure in equilibrium with ambient pressure CO_2. Consistently, the simulated STM image and the corresponding structural model (Fig. 4e and f) show a (3 × 1) structure in agreement with STM measurement (Fig. 4d). From PDOS (Fig. S7), although both chemisorbed and physisorbed CO_2 have unoccupied states responsible for the STM contrast, the highest electronic density is contributed by physisorbed CO_2 which corresponds to the bright dots in the STM image. The chemisorbed CO_2 molecules are located in a lower geometric position, resulting in the dots with darker contrast in the (3 × 1)–CO_2 phase.

Fig. 5 showed that the adsorption energy diagram of CO_2 on ZnO($10\bar{1}0$) varies with a surface coverage of CO_2 and its adsorption state. From above, CO_2 molecules are packed along the [0001] direction, forming chains in the (3 × 1) cell at full coverage. Up to 2/3 ML CO_2 on ZnO($10\bar{1}0$), the total adsorption energies always favor the chemisorption of CO_2, since the transition from physisorbed CO_2 to the chemisorbed CO_2 chain is exothermic by 0.75 eV for 1/3 ML CO_2 from −0.53 eV (Fig. 5a) to −1.28 eV (Fig. 5b) and 0.39 eV for 2/3 ML CO_2 from −1.93 eV (Fig. 5c) and −2.32 eV (Fig. 5d). Yet, further adsorption of CO_2 favors physisorbed CO_2 with a total adsorption energy of −3.11 eV (Fig. 5e), as compared to that for chemisorbed CO_2 at −3.18 eV (Fig. 5f). The structure with 1/3 ML physisorbed CO_2 and 2/3 ML chemisorbed CO_2, as depicted in Fig. 5(e), matches with the (3 × 1) periodicity observed by STM, whereas the 1 ML chemisorption structure (Fig. 5f) displays the (1 × 1) periodicity. Further, the decrease of adsorption energy for chemisorbed CO_2 with increasing coverage is evidenced by the reducing differential adsorption energy of −1.04 eV for the second CO_2 chain, indicating a repulsive interaction between neighboring chemisorbed CO_2 along the [$1\bar{2}10$] direction. On the other hand, the co-adsorption energy for the physisorbed and chemisorbed CO_2 molecules is −1.93 eV (Fig. 5c), and more negative than the sum of respective adsorption energies for physisorbed or chemisorbed CO_2 (Fig. 5a, b), indicating an attractive interaction between physisorbed and chemisorbed CO_2 molecules along the [$1\bar{2}10$] direction. Gibbs free energies were further calculated to identify the adsorption structure of CO_2 at varying temperatures and pressures (Fig. S8) and confirmed the formation of (3 × 1)–CO_2 structure under AP conditions at 300 K and the formation of (2 × 1)–CO_2 structure in UHV.

The dynamic structural transition from (2 × 1)–CO_2, 1/2 ML chemisorbed CO_2, to (3 × 1)–CO_2, 2/3 ML chemisorbed CO_2 + 1/3 ML physisorbed CO_2, might originate from the electrostatic attractive interaction between physisorbed and chemisorbed CO_2 molecules. The surface dipole moments of physisorbed (Fig. 5a) and chemisorbed CO_2 (Fig. 5b) were calculated by $\mu = (1/12\pi)A\Delta\Phi/\Theta$, [56] where A is the area in Å^2 per (1 × 1) surface unit cell, $\Delta\Phi$ is the work-function change in eV and Θ is the surface coverage of CO_2. While the surface dipole moment increased significantly from physisorbed CO_2 (−0.7 Debye) to chemisorbed CO_2 (2.1 Debye), the direction of surface dipoles formed by chemisorbed CO_2 is opposite to that of physisorbed CO_2, suggesting an attractive interaction between chemisorbed and physisorbed CO_2 (Fig. 5c). In addition, the chain of physisorbed CO_2 inserted between chains of chemisorbed CO_2 (Fig. 5e) will not only cause the attractive interaction between physisorbed and chemisorbed CO_2, but also shield the dipole repulsion between neighboring chains of chemisorbed CO_2, as such both the physisorption and chemisorption of CO_2 are further enhanced. This change can be seen further from decreasing height of 2.46 Å for the first physisorbed CO_2 chain (Fig. 5a) to 2.32 Å (Fig. 5c) and 2.24 Å for the sec-

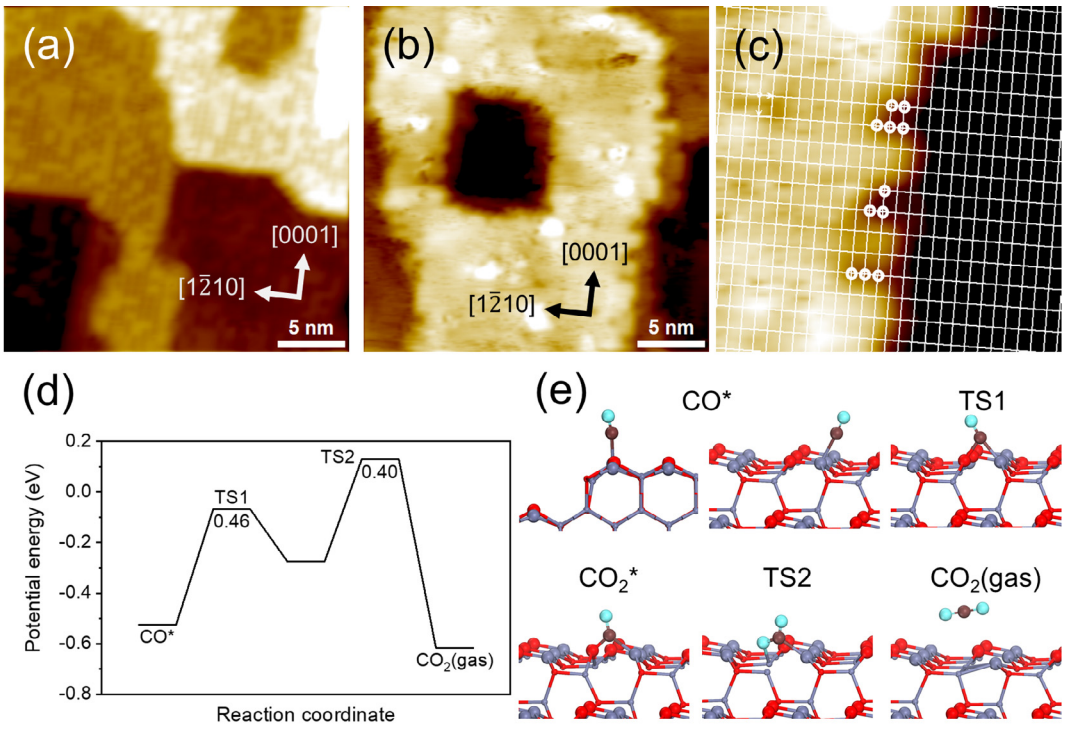

Fig. 3. Reaction of CO on ZnO(10$\bar{1}$0) under ambient conditions. (a) Large-scale STM images of ZnO(10$\bar{1}$0) in 1 mbar CO after being annealed at 500 K. The STM scanning was performed after cooling down to room temperature. (b, c) STM images of step sites of ZnO(10$\bar{1}$0) which was exposed to 1 mbar CO at 500 K and then annealed at 500 K in UHV to remove adsorbates. The hollow circles in (c) represent missing Zn-O pairs at step sites. The grids represent Zn lattice. (d) The calculated potential energy surface and (e) the optimized configurations of reaction intermediates and transition state structures of <0001> step reduced by CO. Scanning parameters: (a) U = 2.5 V, I_t = 130 pA; (b and c) U = 2.5 V, I_t = 100 pA. Gray, red, green and brown spheres represent Zn, lattice O, O in adsorbents and C atoms, respectively. (For interpretation of the references to colour in this figure legend, the reader is referred to the web version of this article.)

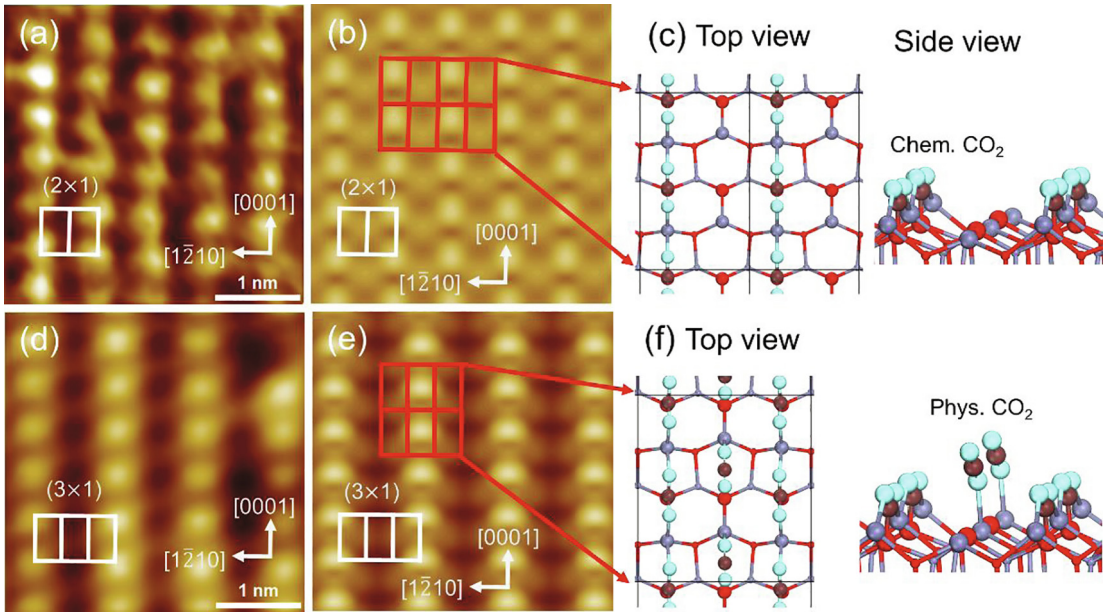

Fig. 4. Adsorption of CO_2 on ZnO(10$\bar{1}$0) from UHV to ambient conditions. (a–f) Atomically-resolved STM images and STM simulation of the adsorbate structures of CO_2 on ZnO(10$\bar{1}$0). (a) A (2 × 1) STM image observed in 8 × 10^{-8} mbar CO_2 at room temperature. The white rectangles represent surface Zn lattice. (b) Simulated STM image, and (c) the optimized (2 × 1)-1/2 ML CO_2 structure by DFT, where CO_2 chemisorbs on ZnO(10$\bar{1}$0) forming tridentate carbonate species. (d) A (3 × 1) STM image observed on ZnO(10$\bar{1}$0) in 3 mbar CO_2 at room temperature. (e) Simulated STM image and (f) the optimized (3 × 1)-1 ML CO_2 structure by DFT, including 2/3 ML chemisorbed CO_2 plus 1/3 ML physisorbed CO_2. Scanning parameters: (a) U = 0.7 V, I_t = 240 pA; (d) U = 2.7 V, I_t = 140 pA. Gray, red, green and brown spheres represent Zn, lattice O, O in adsorbents and C atoms, respectively. (For interpretation of the references to colour in this figure legend, the reader is referred to the web version of this article.)

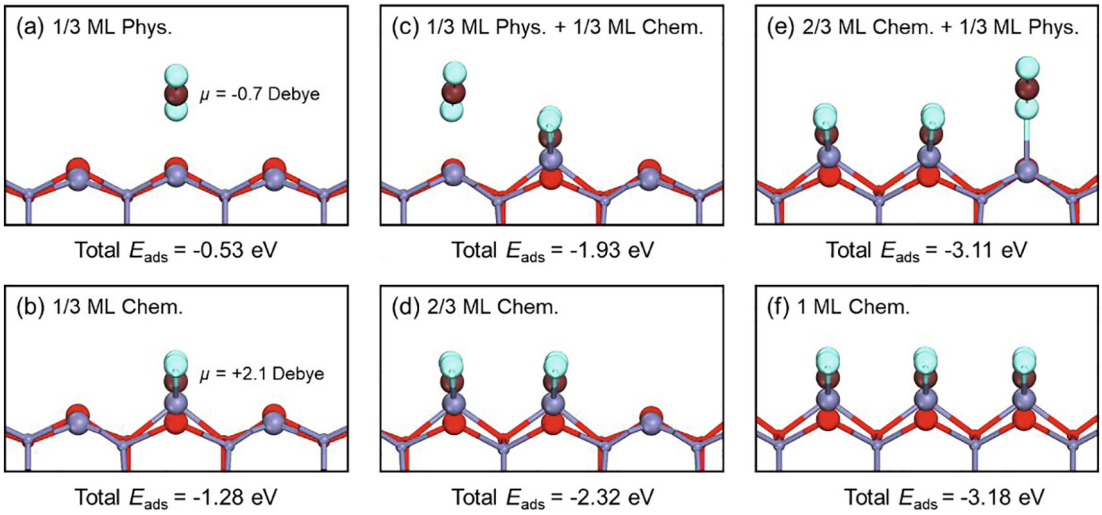

Fig. 5. Optimized adsorption configurations and the total adsorption energies of CO_2 on the ZnO(10$\bar{1}$0) surface. (a) 1/3 ML physisorbed CO_2, (b) 1/3 ML chemisorbed CO_2, (c) 1/3 ML physisorbed CO_2 plus 1/3 ML chemisorbed CO_2 plus, (d) 2/3 ML chemisorbed CO_2, (e) 1/3 ML physisorbed CO_2 plus 2/3 ML chemisorbed CO_2, (f) 1 ML chemisorbed CO_2. Gray, red, green and brown spheres represent Zn, lattice O, O in adsorbents and C atoms, respectively. (For interpretation of the references to colour in this figure legend, the reader is referred to the web version of this article.)

ond (Fig. 5c) and third chains (Fig. 5e) of physisorbed CO_2. The adsorption of CO_2 becomes more exothermic with increasing CO_2 coverage until the surface is fully covered by CO_2. Thus, at 1 ML, the most stable configuration of CO_2 adsorption is the surface with 1/3 ML of physisorbed CO_2 and 2/3 ML of chemisorbed CO_2.

AP-XPS measurements (Fig. S9) also showed that the exposure of 1 mbar CO_2 at 300 K leads to strong chemisorption of CO_2, i.e. the formation of tridentate carbonate species with a surface coverage much higher than that caused by CO exposure under similar conditions. Interestingly, AP-STM study (Fig. S10) also showed that CO_2 did not adsorb on surface defects of ZnO(10$\bar{1}$0), where the adsorption of small molecules was often strengthened at defect sites of reducible oxides. This could be attributed to the different nature of surface defect sites of ZnO, as a non-reducible oxide. On ZnO(10$\bar{1}$0), both Zn and O atoms are missing at the defect sites, whereas the point defects are typically oxygen vacancies on reducible oxides. Thus, the presence of low coordinating metal cations is essential for the adsorption and activation of reactant molecules.

4 Conclusions

We combined AP-STM, AP-XPS and DFT calculations to study the adsorption and reaction of CO and CO_2 on ZnO(10$\bar{1}$0). Despite the weak interaction between CO and ZnO, physisorption of CO on ZnO(10$\bar{1}$0) could be observed in ambient CO gas and form an ordered (2 × 1)–CO structure at 300 K, which would desorb completely upon the evacuation of CO gas. Interestingly, the adsorption of CO also led to simultaneous reaction with ZnO at 300 K to form CO_2. The etching of step edges of ZnO(10$\bar{1}$0) was evident for the reaction between lattice oxygen and CO. In comparison, chemisorption of CO_2 on ZnO(10$\bar{1}$0) occurs readily in UHV and forms tridentate carbonate species. Yet, the co-presence of physisorbed CO_2 under ambient conditions could alter the locations of chemisorbed CO_2, enhance its adsorption and lead to the formation of a new adsorbate structure, (3 × 1)–CO_2, on ZnO(10$\bar{1}$0). Overall, our study showed that the collective interaction of physisorbed molecules results in dynamic chemical processes on the oxide surface, which are not observed in UHV. Our study has also brought molecular insight into the activation of C1 molecules on ZnO surfaces under realistic reaction conditions.

Declaration of Competing Interest

The authors declare that they have no known competing financial interests or personal relationships that could have appeared to influence the work reported in this paper.

Acknowledgments

This work was financially supported by the Ministry of Science and Technology of China (2018YFA0208603) and the National Natural Science Foundation of China (21972144, 91545204, 91845109, 91945302, 22002090), the Chinese Academy of Sciences (QYZDJ-SSW-SLH054), the K. C. Wong Education (GJTD-2020-15), and used high-performance computational resources provided by University of Science and Technology of China. Part of this research used SPECS AP-XPS instruments, which is supported by ME2 project under contract no. 11227902 from National Natural Science Foundation of China.

Appendix A. Supplementary data

Supplementary data to this article can be found online at https://doi.org/10.1016/j.jechem.2022.03.009.

References

[1] M.V. Kovalenko, L. Manna, A. Cabot, Z. Hens, D.V. Talapin, C.R. Kagan, V.I. Klimov, A.L. Rogach, P. Reiss, D.J. Milliron, P. Guyot-Sionnnest, G. Konstantatos, W.J. Parak, T. Hyeon, B.A. Korgel, C.B. Murray, W. Heiss, ACS Nano (2015) 1012–1057.
[2] F.M. Pinto, V.Y. Suzuki, R.C. Silva, F.A. La Porta, Front. Mater. 6 (2019) 260.
[3] R.A. van Santen, I. Tranca, E.J.M. Hensen, Catal. Today 244 (2015) 63–84.
[4] D.J. Driscoll, W. Martir, J.X. Wang, J.H. Lunsford, J. Am. Chem. Soc. 107 (1985) 58–63.
[5] Y. Martynova, B.H. Liu, M.E. McBriarty, I.M.N. Groot, M.J. Bedzyk, S. Shaikhutdinov, H.J. Freund, J. Catal. 301 (2013) 227–232.
[6] G.S. Parkinson, U. Diebold, in: Adsorption on Metal Oxide Surfaces, Wiley-VCH Verlag GmbH & Co. KGaA, Weinheim, 2016, pp. 793–817.
[7] M.A. van Spronsen, J.W.M. Frenken, I.M.N. Groot, Nat. Commun. 8 (2017) 429.
[8] B. Boeller, P. Zeller, S. Guenther, J. Wintterlin, ACS Catal. 10 (2020) 12156–12166.
[9] B. Boeller, K.M. Durner, J. Wintterlin, Nat. Catal. 2 (2019) 1027–1034.
[10] M. Salmeron, B. Eren, Chem. Rev. 121 (2021) 962–1006.
[11] F. Tao, S. Dag, L.-W. Wang, Z. Liu, D.R. Butcher, H. Bluhm, M. Salmeron, G.A. Somorjai, Science 327 (2010) 850–853.
[12] F. Tao, M. Salmeron, Science 331 (2011) 171–174.

[13] J. Balajka, M.A. Hines, W.J.I. DeBenedetti, M. Komora, J. Pavelec, M. Schmid, U. Diebold, Science 361 (2018) 786–789.
[14] F. Yang, D.W. Goodman, in: In Situ STM Studies of Model Catalysts, Wiley-VCH Verlag GmbH & Co. KGaA, Weinheim, 2009, pp. 55–95.
[15] M. Setvín, U. Aschauer, P. Scheiber, Y.-F. Li, W. Hou, M. Schmid, A. Selloni, U. Diebold, Science 341 (2013) 988–991.
[16] A. Kolodziejczak-Radzimska, T. Jesionowski, Materials 7 (2014) 2833–2881.
[17] J.C. Slaa, J.G. Vanommen, J.R.H. Ross, Catal. Today 15 (1992) 129–148.
[18] F. Jiao, J. Li, X. Pan, J. Xiao, H. Li, H. Ma, M. Wei, Y. Pan, Z. Zhou, M. Li, S. Miao, J. Li, Y. Zhu, D. Xiao, T. He, J. Yang, F. Qi, Q. Fu, X. Bao, Science 351 (2016) 1065–1068.
[19] A. Haryanto, S. Fernando, N. Murali, S. Adhikari, Energ. Fuel. 19 (2005) 2098–2106.
[20] J.A. Rodriguez, P. Liu, J. Hrbek, J. Evans, M. Perez, Angew. Chem.-Int. Edit. 46 (2007) 1329–1332.
[21] T.M. Parker, N.G. Condon, R. Lindsay, F.M. Leibsle, G. Thornton, Surf. Sci. 415 (1998) 1046–1050.
[22] U. Diebold, L.V. Koplitz, O. Dulub, Appl. Surf. Sci. 237 (2004) 336–342.
[23] Y. Wang, R. Kováčik, B. Meyer, K. Kotsis, D. Stodt, V. Staemmler, H. Qiu, F. Traeger, D. Langenberg, M. Muhler, C. Wöll, Angew. Chem. Int. Ed. 46 (2007) 5624–5627.
[24] Y. Cao, M. Yu, S. Qi, T. Wang, S. Huang, S. Hu, M. Xu, S. Yan, Sci. Rep. 7 (2017) 43442.
[25] M. Buchholz, P.G. Weidler, F. Bebensee, A. Nefedov, C. Woll, Phys. Chem. Chem. Phys. 16 (2014) 1672–1678.
[26] M. Buchholz, X.J. Yu, C.W. Yang, S. Heissler, A. Nefedov, Y.M. Wang, C. Woll, Surf. Sci. 652 (2016) 247–252.
[27] C. Woll, Prog. Surf. Sci. 82 (2007) 55–120.
[28] Y. Wang, B. Meyer, X. Yin, M. Kunat, D. Langenberg, F. Traeger, A. Birkner, C. Woll, Phys. Rev. Lett. 95 (2005) 266104.
[29] D. Scarano, G. Spoto, S. Bordiga, A. Zecchina, C. Lamberti, Surf. Sci. 276 (1992) 281–298.
[30] H. Chen, L. Lin, Y.F. Li, R. Wang, Z.M. Gong, Y. Cui, Y.S. Li, Y. Liu, X.F. Zhao, W.G. Huang, Q. Fu, F. Yang, X.H. Bao, ACS Catal. 9 (2019) 1373–1382.
[31] Q. Liu, Y. Han, Y.J. Cao, X.B. Li, W.G. Huang, Y. Yu, F. Yang, X.H. Bao, Y.M. Li, Z. Liu, Acta Phys. -Chim. Sin. 34 (2018) 1366–1372.
[32] G. Kresse, J. Furthmüller, Phys. Rev. B 54 (1996) 11169–11186.
[33] P.E. Blöchl, Phys. Rev. B 50 (1994) 17953–17979.
[34] G. Kresse, D. Joubert, Phys. Rev. B 59 (1999) 1758–1775.
[35] J. Klimeš, D.R. Bowler, A. Michaelides, Phys. Rev. B 83 (2011) 195131.
[36] J.P. Perdew, K. Burke, M. Ernzerhof, Phys. Rev. Lett. 77 (1996) 3865–3868.
[37] X.-K. Gu, B. Qiao, C.-Q. Huang, W.-C. Ding, K. Sun, E. Zhan, T. Zhang, J. Liu, W.-X. Li, ACS Catal. 4 (2014) 3886–3890.
[38] X.-K. Gu, C.-Q. Huang, W.-X. Li, Catal. Sci. Technol. 7 (2017) 4294–4301.
[39] R. Escudero, R. Escamilla, Solid State Commun. 151 (2011) 97–101.
[40] S.C. Abrahams, J.L. Bernstein, Acta Crystallogr. Sect. B 25 (1969) 1233–1236.
[41] G. Henkelman, H. Jónsson, J. Chem. Phys. 113 (2000) 9978–9985.
[42] G. Henkelman, B.P. Uberuaga, H. Jónsson, J. Chem. Phys. 113 (2000) 9901–9904.
[43] J. Tersoff, D.R. Hamann, Phys. Rev. Lett. 50 (1983) 1998–2001.
[44] J. Tersoff, D.R. Hamann, Phys. Rev. B 31 (1985) 805–813.
[45] B. Wang, X. Ma, M. Caffio, R. Schaub, W.-X. Li, Nano Lett. 11 (2011) 424–430.
[46] W.A. Hofer, Prog. Surf. Sci. 71 (2003) 147–183.
[47] H. Wang, X. Zhao, C. Huang, X. Jin, D. Wei, D. Dai, Z. Ma, W.-X. Li, X. Yang, J. Phys. Chem. Lett. 10 (2019) 3352–3358.
[48] D. Wei, X. Jin, C. Huang, D. Dai, Z. Ma, W.-X. Li, X. Yang, J. Phys. Chem. C 119 (2015) 17748–17754.
[49] R.R. Gay, M.H. Nodine, V.E. Henrich, H.J. Zeiger, E.I. Solomon, J. Am. Chem. Soc. 102 (1980) 6752–6761.
[50] H. Shi, H. Yuan, S.Q. Ruan, W.Y. Wang, Z. Li, Z.Y. Li, X. Shao, J. Phys. Chem. C 122 (2018) 8919–8924.
[51] S. Wendt, J. Matthiesen, R. Schaub, E.K. Vestergaard, E. Laegsgaard, F. Besenbacher, B. Hammer, Phys. Rev. Lett. 96 (2006) 066107.
[52] X.L. Yin, A. Birkner, K. Hanel, T. Lober, U. Kohler, C. Woll, Phys. Chem. Chem. Phys. 8 (2006) 1477–1481.
[53] Y.J. Cao, J. Luo, W.G. Huang, Y.J. Ling, J.F. Zhu, W.X. Li, F. Yang, X.H. Bao, J. Chem. Phys. 152 (2020) 8.
[54] H. Shi, S.Q. Ruan, H.H. Liu, L. Wang, W.Y. Wang, X.G. Ren, B. Wang, K. Wu, X. Shao, J. Phys. Chem. C 120 (2016) 23669–23674.
[55] Z.Z. Lai, N.L. Sun, J.M. Jin, J.F. Chen, H.F. Wang, P. Hu, ACS Catal. 11 (2021) 12977–12988.
[56] W.-X. Li, C. Stampfl, M. Scheffler, Phys. Rev. B 65 (2002) 075407.